Temperature Effects in Adsorption of a Primitive Model Electrolyte in Disordered Quenched Media: Predictions of the Replica OZ/HNC Approximation

V. Vlachy,*,† H. Dominguez,‡ and O. Pizio‡

Faculty of Chemistry and Chemical Technology, University of Ljubljana, Aškerčeva 5, 1000 Ljubljana, Slovenia, and Instituto de Quımica de la UNAM, Circuito Exterior, Coyoacán 04510, México D.F.

Received: April 30, 2003; In Final Form: October 19, 2003

A theoretical study of a quenched−annealed system where both components were modeled as charge symmetric +1:−1 primitive model electrolytes is presented. The adsorbed model electrolyte, mimicking lithium chloride solution, was assumed to be in thermodynamic equilibrium with an external reservoir of the same electrolyte. This partly quenched system was studied by applying the replica Ornstein−Zernike (ROZ) integral equation in the hypernetted chain (HNC) approximation and the grand canonical Monte Carlo technique. The effects of the concentration of matrix ions, pre-quenching conditions, and the electrolyte and solvent conditions on the adsorption of electrolyte were examined. The results indicate that the mean activity coefficient of the adsorbed electrolyte may differ substantially from the value of the corresponding quantity in the equilibrium bulk solution. The concentration of the annealed electrolyte in the matrix can be higher (sorption) or lower (rejection) than the corresponding equilibrium bulk concentration, depending on conditions of matrix preparation and on the temperature of adsorption. An important observation of this study is that the ROZ/HNC approximation can be solved for very high couplings, i.e., we can obtain valid results in the region of parameters where the regular OZ/HNC, applied to the equivalent bulk electrolyte solution, fails to converge. The agreement between the computer simulations and ROZ/HNC results for the adsorption isotherms is good.

1. Introduction

The equilibrium statistical thermodynamics of fluids in heterogeneous media is a topic of considerable practical and scientific importance. These systems can be found in industrial applications such as heterogeneous catalysis, separation processes, ion-exchange, and others. Theoretically, disordered porous materials filled with liquid may be considered as partly quenched systems, i.e., materials in which some of the degrees of freedom are quenched, and others are annealed. The ensemble average used to calculate the thermodynamic averages in such systems becomes a double ensemble average: first over the annealed degrees of freedom, and then over all the possible values of the quenched variables. In this respect annealed−quenched systems differ from regular mixtures. The computer simulations of such systems are necessarily time-consuming and development of more analytical theories is clearly warranted.

In the past decade a new theoretical approach has been developed by adaptation of ideas from liquid-state statistical mechanics.[1−11] Extensive lists of references, together with discussion of important theoretical and experimental developments in this area of research, are given in recent review papers.[12−14] Partly quenched systems seem to have been first studied by Madden and Glandt,[1,2] who considered a fluid introduced into a random structure that was statistically homogeneous on all but molecular length scales. Using methods of topological reduction, they developed the Ornstein−Zernike integral equations for the correlation functions. In an important contribution Given and Stell[3−5] applied the so-called continuum replica method, which involves relating a partly quenched system to a fully equilibrated system called the replicated system, to derive the so-called replica Ornstein−Zernike (ROZ) equation. The ROZ theory has been successfully applied so far to several model systems.[12−14] Partly quenched systems containing particles interacting via the Coulomb interaction[15−18] have also been studied. Bratko and Chakraborty[16] utilized Monte Carlo simulations to investigate the behavior of a dilute ionic fluid in a quenched disordered medium with ionic obstacles. The structure of the medium was assumed to correspond to that of an ionic fluid equilibrated at a certain pre-quenching temperature and dielectric permittivity, different from the corresponding values under the conditions of observation.

In several recent contributions from our group the replica Ornstein−Zernike theory was applied to study the adsorption of a model ionic fluid in a disordered medium with ionic[19−23] or neutral[24,25] obstacles. In these studies the matrix and the adsorbed fluid were treated in the primitive model approximation, i.e., the ions were modeled as charged hard spheres embedded in a dielectric continuum. The matrix, represented as an electroneutral system of positively and negatively charged hard spheres,[22,23] was assumed to be formed by a rapid quench of the electrolyte solution being equilibrated at temperature T_0, and characterized by dielectric constant ϵ_0. The assumption was that the distribution of matrix particles corresponds to an equilibrium state of the ionic fluid of concentration c_0 at temperature T_0. The annealed component, also pictured as a primitive model electrolyte in a solvent with ϵ, was than assumed to be distributed within the matrix at the temperature of observation T_1. The adsorbed electrolyte is assumed to be in equilibrium with an external reservoir of the same model electrolyte at this temperature; the condition of equilibrium required all permeable ions to have equal chemical potential in both "phases". Limited comparison of the ROZ/HNC calculations with the grand canonical Monte Carlo data indicated that

* Corresponding author.
† University of Ljubljana.
‡ Instituto de Quımica de la UNAM.

10.1021/jp035166b CCC: $27.50
Published on Web 12/16/2003

the theory provides semiquantitatively correct predictions for the equilibrium distribution of a +1:−1 electrolyte between the matrix and the external solution for the conditions (temperature, dielectric constant) examined in refs 22 and 23.

The present contribution is a continuation of our studies described above. It represents further investigation of the applicability of the replica OZ theory in the HNC approximation to describe partly quenched systems with charged obstacles. In addition, the ROZ/HNC results are complemented by the grand canonical Monte Carlo simulation of the same system. Of considerable interest is to learn how the presence of obstacles affects the structure and thermodynamics of the adsorbed electrolyte. There are two properties which are of central interest for this study. One is the chemical potential of the annealed electrolyte, which actually determines the equilibrium between the external electrolyte solution and the adsorbed electrolyte. This quantity is of primary importance for determination of the equilibrium distribution of electrolyte between the porous medium and the bulk phase. The second property of interest is the so-called osmotic compressibility, this quantity reflects the stability of the adsorbed electrolyte. The study presented here complements our previous research in the following aspect: The ROZ/HNC calculation is extended into the range of parameters (T_1, ϵ) where electrostatic interactions are very strong. This is the range of parameters where the regular HNC approximation, when applied to a bulk (unperturbed) electrolyte solution, may not provide convergent solutions. For the specific model used in this work, we explored the influence of the temperature of matrix preparation and its concentration, as well as the effects of temperature of adsorption. The conclusion is that the HNC approximation, when applied in the framework of the replica formalism, can be solved for stronger couplings than the regular HNC approximation, which applies to unperturbed electrolytes. For example, the HNC approximation for a model electrolyte could not be solved for the reduced temperature $T_1 = 60.15$ K in the whole concentration range, while the replica HNC equations for the adsorbed electrolyte give a convergent solution for this and even lower temperatures. Moreover, these results are in fair agreement with the new computer simulations of these systems.

2. Model System

The model system under investigation, for details see also ref 20, is composed of two subsystems. The first subsystem is a quenched ionic fluid, called the matrix, and the second is an annealed electrolyte, which thermally equilibrates in the presence of matrix particles. Note that the matrix particles do not respond to the presence of the annealed fluid. The notation is as usual in these studies: the superscripts 0 and 1 correspond to the matrix and the annealed fluid species, respectively. The matrix, represented as an electroneutral system of positively and negatively charged hard spheres with charges ez_+^0 and ez_-^0 ($z_+^0 = 1$, $z_-^0 = -1$), is assumed to be formed as follows: at a certain temperature T_0 the electrolyte solution (ϵ_0) is subjected to a rapid quench. It is assumed that the spatial distribution of matrix ions does not change during the quench, and is therefore completely determined by T_0.

In the present work we investigate the case where the matrix is formed from a model +1:−1 electrolyte. The diameters of ions were chosen to be $\sigma_+^0 = \sigma_-^0 = 4.25$ Å as in some previous studies.[16,20] The matrix ions with the number concentrations ρ_+^0 and ρ_-^0, respectively, are immersed in a dielectric continuum with a dielectric constant ϵ_0. The interaction pair potential for such an example is:

$$U_{ij}^{00}(r) = \begin{cases} \infty & r < (\sigma_+^0 + \sigma_-^0)/2 \\ e^2 z_i^0 z_j^0/\epsilon_0 r & r \geq (\sigma_+^0 + \sigma_-^0)/2 \end{cases} \quad (1)$$

where i and j assume values + and −.

The model for the annealed electrolyte is similar to that of the matrix; it corresponds to an electroneutral system of charged hard spheres with charges ez_+^1 and ez_-^1 ($z_+^1 = 1$, $z_-^1 = -1$) and diameters σ_+^1 and σ_-^1. The sizes of the ions were chosen to mimic LiCl solution:[26] $\sigma_{Li}^1 = 5.43$ Å and $\sigma_{Cl}^1 = 3.62$ Å. These diameters are adjusted to the mean-spherical description of the primitive model electrolyte and yield good agreement with experimental data.[26] The total ionic number concentration of annealed species is equal to $\rho_1 = \rho_+^1 + \rho_-^1$, and the solvent is modeled as a dielectric continuum with constant ϵ. Adsorption was studied at conditions T_1, ϵ which are different from the conditions T_0, ϵ_0 under which the matrix was equilibrated. The fluid−fluid $U_{ij}^{11}(r)$ and the fluid−matrix $U_{ij}^{10}(r)$ pair potentials are defined as:

$$U_{ij}^{11}(r) = \begin{cases} \infty & r < (\sigma_i^1 + \sigma_j^1)/2 \\ e^2 z_i^1 z_j^1/\epsilon r & r \geq (\sigma_i^1 + \sigma_j^1)/2 \end{cases} \quad (2)$$

and

$$U_{ij}^{10}(r) = \begin{cases} \infty & r < (\sigma_i^1 + \sigma_j^0)/2 \\ e^2 z_i^1 z_j^0/\epsilon r, & r \geq (\sigma_i^1 + \sigma_j^0)/2 \end{cases} \quad (3)$$

Note also that other solvent averaged potential functions, containing contributions from the overlap of the solvation shells (see, for example, ref 27) may easily be incorporated into the replica formalism. The numerical values of thermodynamic parameters studied in this work may depend on the details of the solvent-averaged potential especially at higher electrolyte concentrations, but the trends observed in calculations are expected to be the same.

In this paper most of the calculations apply to a matrix formed at $T_0 = 298.15$ K and in a solvent with $\epsilon_0 = 78.54$. The structural and thermodynamic properties of the annealed electrolyte were examined for a set of T_1 and ϵ values. Note that the two parameters T_1 and ϵ can be combined into one. For simplicity of presentation we choose $\epsilon = \epsilon_0$, so the strength of interaction between the molecules of annealed fluid and the annealed fluid−matrix ions is reflected solely in the value of T_1.

3. Replica Ornstein−Zernike Theory

To obtain the properties of the model system we utilize the replica Ornstein−Zernike equations in the form:[20]

$$\mathbf{H}^{00} - \mathbf{C}^{00} = \mathbf{C}^{00} \otimes \rho^0 \mathbf{H}^{00}$$

$$\mathbf{H}^{10} - \mathbf{C}^{10} = \mathbf{C}^{10} \otimes \rho^0 \mathbf{H}^{00} + \mathbf{C}^{11} \otimes \rho^1 \mathbf{H}^{10} - \mathbf{C}^{12} \otimes \rho^1 \mathbf{H}^{10}$$

$$\mathbf{H}^{11} - \mathbf{C}^{11} = \mathbf{C}^{10} \otimes \rho^0 \mathbf{H}^{01} + \mathbf{C}^{11} \otimes \rho^0 \mathbf{H}^{11} - \mathbf{C}^{12} \otimes \rho^1 \mathbf{H}^{21}$$

$$\mathbf{H}^{12} - \mathbf{C}^{12} = \mathbf{C}^{10} \otimes \rho^0 \mathbf{H}^{01} + \mathbf{C}^{11} \otimes \rho^1 \mathbf{H}^{12} + \mathbf{C}^{12} \otimes \rho^1 \mathbf{H}^{11} - 2\mathbf{C}^{12} \otimes \rho^1 \mathbf{H}^{21} \quad (4)$$

where ⊗ denotes convolution. The first equation in this set describes the matrix subsystem. Since the electrolyte solutions

are two-component systems containing cations (+) and anions (−) ρ^i has the form ($i = 0,1$):

$$\begin{pmatrix} \rho_+^i & 0 \\ 0 & \rho_-^i \end{pmatrix} \tag{5}$$

Further, $\mathbf{H}^{mn}$ as well as $\mathbf{C}^{mn}$ are matrices of dimension 2×2, containing $++$, $+-$ $(-+)$, and $--$ functions. The annealed fluid correlation functions $\mathbf{H}^{11}$ and $\mathbf{C}^{11}$ are divided into connecting and blocking parts.[4,20] Blocking parts are denoted as $\mathbf{H}^{12}$ and $\mathbf{C}^{12}$. As explained elsewhere[1,2,4] the connected functions, for example, $\mathbf{H}^{11} - \mathbf{H}^{12}$, account for the correlation between a pair of fluid particles propagating via other fluid particles, and the blocking functions account for the correlations between fluid particles "blocked" from each other by the matrix particles.

To solve the set of integral equations written above, we need to assume so-called closure conditions. For electrolyte solutions the so-called hypernetted chain (HNC) closure is known for its accuracy and therefore often used.[28,29] A disadvantage of the HNC theory is the limited convergence obtained for highly coupled systems.[30] In this study we apply the HNC closure condition in the form:

$$\mathbf{C}^{mn}(r) = \mathrm{e}^{[-\beta_1 \mathbf{U}mn(r) + \Gamma mn(r)]} - 1 - \Gamma^{mn}(r)$$

$$\mathbf{C}^{12}(r) = \mathrm{e}^{\Gamma^{12}}(r) - 1 - \Gamma^{12}(r) \tag{6}$$

In this equation $\Gamma^{mn} = \mathbf{H}^{mn} - \mathbf{C}^{mn}$, and the superscripts m, n assume values 0 and 1. Further, $\mathbf{U}^{mn}$ are the matrices of interparticle pair potentials, and $\beta_1 = 1/k_B T_1$, where k_B is the Boltzmann constant.[20]

4. Renormalized Form of ROZ Equations

The set of equations given in the previous section is not yet in a form suitable for numerical solution. To avoid divergence of the integrals with potentials proportional to r^{-1}, we need to apply a suitable renormalization scheme. In analogy with studies of bulk electrolyte solutions, we split the correlation functions $\mathbf{C}$ and $\mathbf{H}$ into short-range (denoted by the subscript (s)) and long-range parts:[20]

$$\mathbf{C}^{mn}(r) = \mathbf{C}_{(s)}^{mn}(r) + \Phi^{mn}(r)$$

$$\mathbf{C}^{0m}(r) = \mathbf{C}_{(s)}^{0m}(r) + \Phi^{0m}(r)$$

$$\mathbf{C}^{12}(r) = \mathbf{C}_{(s)}^{12}(r) \tag{7}$$

and

$$\mathbf{H}^{mn}(r) = \mathbf{H}_{(s)}^{mn}(r) + \mathbf{q}^{mn}(r) \tag{8}$$

where the superscripts m, n assume the values 0, 1, 2. Further, $\mathbf{C}^{22}(r) = \mathbf{C}^{11}(r)$, $\mathbf{C}^{01}(r) = \mathbf{C}^{02}(r)$, $\mathbf{H}^{22}(r) = \mathbf{H}^{11}(r)$, and $\Phi^{22}(r) = \Phi^{11}(r)$. The particles belonging to different replicas do not interact and therefore $\Phi^{12}(r) = \mathbf{0}$. The elements $\varphi_{ij}^{mn}(r)$ of the matrix $\Phi^{mn}(r)$ are given in the form of Coulomb interactions[20]

$$\varphi_{ij}^{mn}(r) = -e^2 z_i^m z_j^n / k_B \epsilon T_1 r$$

$$\varphi_{ij}^{00}(r) = -e^2 z_i^0 z_j^0 / k_B \epsilon_0 T_0 r \tag{9}$$

and the functions $\mathbf{q}^{mn}(r)$ are chosen to satisfy the following equations:[19]

$$\mathbf{q}^{00} - \Phi^{00} = \Phi^{00} \otimes \rho^0 \mathbf{q}^{00}$$

$$\mathbf{q}^{10} - \Phi^{10} = \Phi^{10} \otimes \rho^0 \mathbf{q}^{00} + \Phi^{11} \otimes \rho^1 \mathbf{q}^{10}$$

$$\mathbf{q}^{11} - \Phi^{11} = \Phi^{10} \otimes \rho^0 \mathbf{q}^{01} + \Phi^{11} \otimes \rho^1 \mathbf{q}^{11}$$

$$\mathbf{q}^{12} - \Phi^{12} = \Phi^{10} \otimes \rho^0 \mathbf{q}^{01} + \Phi^{11} \otimes \rho^1 \mathbf{q}^{12} \tag{10}$$

Finally, the renormalized ROZ equations read:[20]

$$\mathbf{H}_{(s)}^{00} - \mathbf{C}_{(s)}^{00} = \mathbf{C}_{(s)}^{00} \otimes \rho^0 (\mathbf{H}_{(s)}^{00} + \mathbf{q}^{00}) + \Phi^{00} \otimes \rho^0 \mathbf{H}_{(s)}^{00} \tag{11}$$

$$\mathbf{H}_{(s)}^{10} - \mathbf{C}_{(s)}^{10} = \mathbf{C}_{(s)}^{10} \otimes \rho^0 (\mathbf{H}_{(s)}^{00} + \mathbf{q}^{00}) + \Phi^{10} \otimes \rho^0 \mathbf{H}_{(s)}^{00} + \mathbf{C}_{(s)}^{11} \otimes \rho^1 (\mathbf{H}_{(s)}^{10} + \mathbf{q}^{10}) + \Phi^{11} \otimes \rho^1 \mathbf{H}_{(s)}^{10} - \mathbf{C}_{(s)}^{12} \otimes \rho^1 (\mathbf{H}_{(s)}^{10} + \mathbf{q}^{10})$$

$$\mathbf{H}_{(s)}^{11} - \mathbf{C}_{(s)}^{11} = \mathbf{C}_{(s)}^{10} \otimes \rho^0 (\mathbf{H}_{(s)}^{01} + \mathbf{q}^{01}) + \Phi^{10} \otimes \rho^0 \mathbf{H}_{(s)}^{01} + \mathbf{C}_{(s)}^{11} \otimes \rho^1 (\mathbf{H}_{(s)}^{11} + \mathbf{q}^{11}) + \Phi^{11} \otimes \rho^1 \mathbf{H}_{(s)}^{11} - \mathbf{C}_{(s)}^{12} \otimes \rho^1 (\mathbf{H}_{(s)}^{21} + \mathbf{q}^{21})$$

$$\mathbf{H}_{(s)}^{12} - \mathbf{C}_{(s)}^{12} = \mathbf{C}_{(s)}^{10} \otimes \rho^0 (\mathbf{H}_{(s)}^{01} + \mathbf{q}^{01}) + \Phi^{10} \otimes \rho^0 \mathbf{H}_{(s)}^{01} + \mathbf{C}_{(s)}^{11} \otimes \rho^1 (\mathbf{H}_{(s)}^{12} + \mathbf{q}^{12}) + \Phi^{11} \otimes \rho^1 \mathbf{H}_{(s)}^{12} - \mathbf{C}_{(s)}^{12} \otimes \rho^1 \mathbf{H}^{11} - 2\mathbf{C}_{(s)}^{12} \otimes \rho^1 \mathbf{H}^{21} \tag{12}$$

The integral equations given above (eqs 10 and 11) were solved by direct iteration. Some details of the actual calculation were given in our previous papers.[20,21,24]

5. Expressions for Thermodynamic Properties

In this section we present equations for the thermodynamic properties which can be calculated once the distribution functions are known. The excess internal energy per annealed fluid particle is given by:[20,21,24]

$$\beta_1 E^{ex}/N_1 = \frac{1}{2} \sum_{i=+,-} \sum_{j=+,-} x_i^1 \rho_j^1 \int \mathrm{d}\mathbf{r}\, g_{ij}^{11}(r)\, U_{ij}^{11}(r) + \sum_{i=+,-} \sum_{j=+,-} x_i^1 \rho_j^0 \int \mathrm{d}\mathbf{r}\, g_{ij}^{10}(r)\, U_{ij}^{10}(r) \tag{13}$$

where, as before, $\beta_1 = 1/k_B T_1$. Further, $x_j^1 = \rho_j^1/\rho_1$ is the fraction of particles of species j in the annealed fluid and $N_1 = N_+^1 + N_-^1$.

In this work we focus on the excess chemical potential of the confined electrolyte to evaluate the adsorption isotherms. Namely, the equilibrium distribution of electrolyte between the porous phase and bulk electrolyte can only be calculated if the individual activity coefficients γ_i^1 of all mobile ionic species are known. The activity coefficient of species i is defined as $\ln(\gamma_i^1) = \beta_1 \mu_i^{1,ex}$, where $\mu_i^{1,ex}$ is the corresponding excess chemical potential and for +1:−1 electrolytes $\gamma_\pm^1 = (\gamma_+^1 \gamma_-^1)^{1/2}$. Recently, an expression for $\ln(\gamma_i^1)$ valid within the ROZ/HNC formalism has been proposed (see, for example, ref 23)

$$\ln(\gamma_i^1) = -\sum_{j=+,-} \rho_j^0 \mathbf{c}_{(s)ij}^{10}(0) - \sum_{j=+,-} \rho_j^1 [\mathbf{c}_{(s)ij}^{11}(0) - \mathbf{c}_{(s)ij}^{12}(0)] + 0.5 \sum_{j=+,-} \rho_j^0 \int \mathrm{d}\mathbf{r}\, h_{ij}^{10}(h_{ij}^{10} - c_{ij}^{10}) + 0.5 \sum_{j=+,-} \rho_j^1 \int \mathrm{d}\mathbf{r}\, [h_{ij}^{11}(h_{ij}^{11} - c_{ij}^{11}) - h_{ij}^{12}(h_{ij}^{12} - c_{ij}^{12})] \tag{14}$$

where $\mathbf{c}_{(s)ij}(\mathbf{0})$ denotes the Fourier transform of the short-range part of the direct correlation function at $k = 0$. As shown in our previous study,[23] this approximate expression, in conjunction with the replica OZ/HNC equations, yields good agreement with Monte Carlo data for the state points studied so far.

The other thermodynamic property of special interest for this study is the reduced isothermal compressibility, $[\partial\rho_1/\partial(\beta_1 P)]_T$, defined via the inverse relation:

$$\beta_1\left(\frac{\partial P}{\partial \rho_1}\right)_T = 1 - \rho_1 \sum_{i=+,-} \sum_{j=+,-} x_i^1 x_j^1 \int \mathrm{d}\mathbf{r}\, [c_{(s)ij}^{11}(r) - c_{(s)ij}^{12}(r)] \tag{15}$$

where ρ_1 is the total number concentration of ions. Note that $[\partial\rho_1/\partial(\beta_1 P)]_T$ defines the ratio between the isothermal compressibility of the fluid of interest divided by the ideal gas value. For the bulk electrolyte solutions treated at the McMillan−Mayer level of description (primitive model) this is actually the osmotic compressibility.[31,32] Isothermal compressibility is intimately connected to the concentration fluctuations in the solution[8] and therefore reflects the thermodynamic stability of the system.

6. Numerical Results

We are concerned with the disorder effect on the structure of a charge symmetric +1:−1 electrolyte. The diameters of the annealed electrolyte are chosen, if not stated otherwise, to mimic *LiCl* solutions:[26] $\sigma_{Li}^1 = 5.43$ Å and $\sigma_{Cl}^1 = 3.62$ Å. The product of temperature of observation T_1 and the dielectric constant ϵ is a measure of the strength of interaction. Different $T_1\epsilon$ values were investigated during this study. In the laboratory, this product can be varied simply by changing the solvent (ϵ). For simplicity of presentation the temperature T_1 is chosen as a single variable, keeping $\epsilon = \epsilon_0 = 78.54$ constant. For illustration, $T_1 = 125$ K here corresponds to a +1:−1 electrolyte studied at room temperature but in a solvent with a dielectric constant ≈33. Experimentally this applies to electrolyte solutions in methanol.

The problems associated with the computer simulations of partly quenched ionic systems were explained elsewhere (refs 22 and 23 and the references therein) and will not be repeated here. The configurational properties of an adsorbed fluid must first (for a chosen matrix configuration) be averaged over the annealed degrees of freedom, and then averaged over the matrix configurations. In principle, the second average extends over all possible configurational states of the matrix, but in practice, a small number of equilibrium matrix realizations (two or three) seems to be sufficient.[22,23] In this paper, most of the simulation results have been obtained via the classical minimum image boundary conditions.[33] This approach is considered to be less accurate at higher electrostatic couplings, i.e., for low temperatures, in comparison with the use of the Ewald summation technique.[33] The disadvantage of the latter approach (Ewald method) is that it is very time-consuming. To check our results for the size effects we (i) studied systems with relatively large number of ions (about 12 000), and in several cases (e.g. for $T_1 = 40.15$ and 60.15 K) we also performed the calculations using the Ewald summation technique. The conclusion is that the differences between the "minimum image" and "Ewald" type of calculations are within the numerical uncertainties of the single calculation of the average concentration of adsorbed electrolyte. These uncertainties are from 2 to 4%.

6.1. Characterization of Matrix. As already mentioned the matrix is represented by an equilibrium configuration of the restricted primitive model for a +1:−1 electrolyte as obtained for T_0 and ϵ_0. For all calculations the diameters of matrix particles are chosen to be $\sigma_+^0 = \sigma_-^0 = 4.25$ Å. An example of spatial correlations between the matrix ions is shown in Figure 1. First in panel a we present the results for pair-correlation functions $h_{+-}^{00}(r)$ and $h_{++}^{00}(r)$ for the matrix subsystem at $T_0 = 298.15$ K. The solid lines represent the results for $c_0 = 0.5$ mol/dm^3, and the dashed lines data for a higher matrix concentration equal to 2.0 mol/dm^3. From these graphs we see that in the more concentrated (denser) matrix oppositely charged ions possess a tendency to pair-formation, and therefore a somewhat smaller ability to adsorb fluid ions is expected.

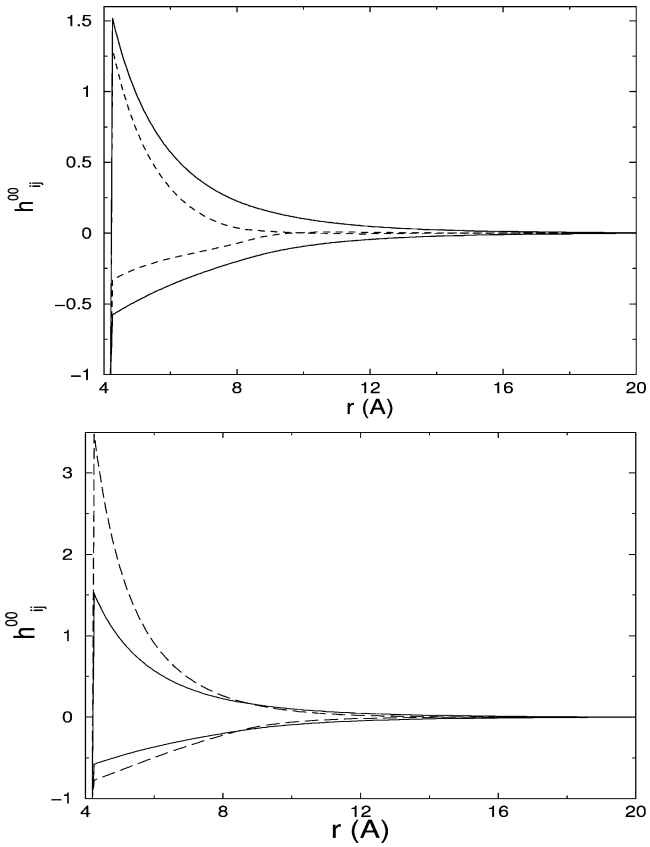

Figure 1. Pair-correlation functions $h_{+-}^{00}(r)$ and $h_{++}^{00}(r)$ for the matrix subsystem ($\sigma_+^0 = \sigma_-^0 = 4.25$ Å). Panel a (top): $c_0 = 0.5$ mol/dm^3 (solid lines), 2.0 mol/dm^3 (dashed lines); $T_0 = 298.15$ K. Panel b (bottom): $T_0 = 298.15$ K (solid lines), $T_0 = 148.15$ K (dashed lines); $c_0 = 0.5$ mol/dm^3.

Next, we wish to discuss the influence of the temperature of matrix preparation T_0 on the spatial correlation between ions. These results are shown in Figure 1b. We consider two matrices of the same concentration, $c_0 = 0.5$ mol/dm^3, one of them prepared at $T_0 = 298.15$ K (shown by solid lines) and the other at the much lower temperature $T_0 = 148.15$ K (dashed lines). The stronger electrostatic interactions in the latter case result in a higher probability of contact between oppositely charged matrix ions, as well as in a shorter range of interionic correlations. As we will see later, the structure of the matrix appreciably influences the thermodynamics of adsorption (see Subsection 6.3).

The analysis of matrix structure, as discussed above, does not include fluid−matrix interactions, and therefore cannot be helpful in understanding all aspects of adsorption. Besides the temperature of preparation T_0, the dimensionless number density, $\rho^*_0 = (\rho_0^+ + \rho_0^-)\sigma_+^{03}$, or packing fraction, $\rho^*_0 = 6\eta_0/\pi$, are important characteristics of the matrix. Alternatively, we can

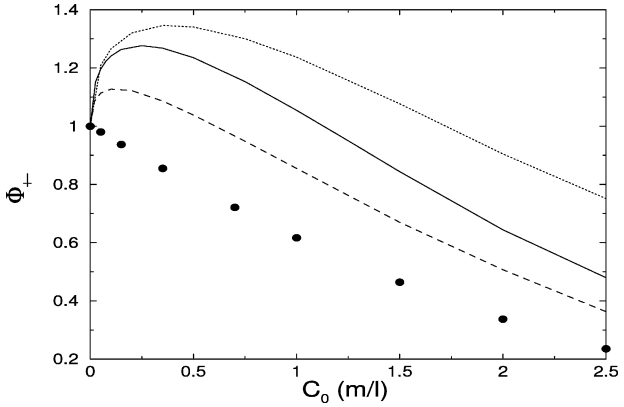

Figure 2. $\Phi_\pm$ as a function of the matrix concentration c_0. Adsorption of the model *LiCl* in hard sphere matrices at $T_1 = 298.15$ K (symbols). Lines denote adsorption in matrices formed from +1:−1 electrolyte ($\sigma_+^0 = \sigma_-^0 = 4.25$ Å): (a) dashed line, model *LiCl* adsorption at $T_1 = 298.15$ K, $T_0 = 148.15$ K, (b) solid line, *LiCl* adsorption at $T_1 = 298.15$ K, $T_0 = 298.15$ K, and (c) dotted line, adsorption of *NaCl* at $T_1 = 298.15$ K, $T_0 = 298.15$ K.

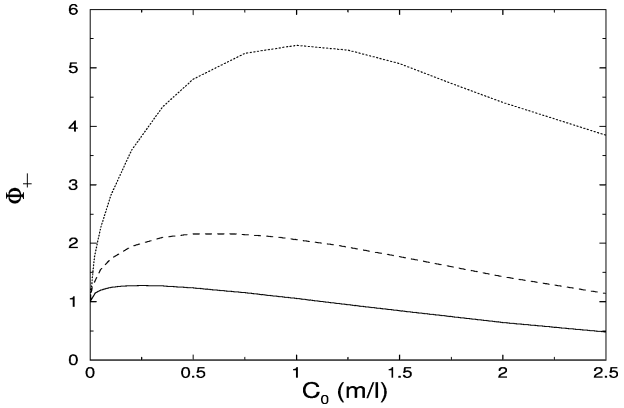

Figure 3. $\Phi_\pm$ as a function of the matrix concentration c_0. Adsorption of the model *LiCl* in hard sphere matrices at $T_1 = 298.15$ K (symbols). Lines denote adsorption in matrices formed from +1:−1 electrolyte ($\sigma_+^0 = \sigma_-^0 = 4.25$ Å): (a) dashed line, model *LiCl* adsorption at $T_1 = 298.15$ K, $T_0 = 148.15$ K, (b) solid line, *LiCl* adsorption at $T_1 = 298.15$ K, $T_0 = 298.15$ K, and (c) dotted line, adsorption of *NaCl* at $T_1 = 298.15$ K, $T_0 = 298.15$ K.

also use a description in terms of electrolyte concentration, $c_0 = \rho_0^+/N_A$, where N_A is Avogadro's number ($\rho_0^+ = \rho_0^-$), rather than of number density. The concentration of ions determines (due to the hard-sphere interaction) the matrix packing fraction, which is related to what is commonly called porosity as $p = 1 - \eta_0$. However, the porosity defined this way does not provide an insight into the affinity of fluid species to matrix obstacles. To characterize the disordered material (matrix) in more detail, we follow the ideas of Van Tassel.[34] The affinity of fluid species to matrix obstacles is reflected in the value of the excess chemical potential of the infinitely diluted fluid particles in a matrix of concentration c_0:

$$\Phi_\pm = \exp\{-\beta_1 \mu_\pm^{1,\mathrm{ex}}(c_1 = 0, c_0)\} \tag{16}$$

where c_1 denotes the concentration of mobile electrolyte. Note that $\Phi_\pm$ is equal to $(\gamma_\pm^1)^{-1}$, where $\gamma_\pm^1$ is the mean activity coefficient of the infinitely diluted annealed electrolyte under these conditions (c_0, T_0, T_1). In this way, $\Phi_\pm$ measures the effects of matrix configuration at a given concentration c_0, and temperature of its preparation, as well as the effects of the fluid−matrix interaction at T_1. To evaluate $\beta_1\mu_\pm^{1,\mathrm{ex}} = \ln(\gamma_\pm^1)$ values for a trace of electrolyte in the matrix, we use the ROZ/HNC expression for the mean activity coefficient given by eq 13 above. In accordance with the standard definition $\gamma_i^1 c_i^1 = a_i^1$, and for the symmetric +1:−1 electrolytes studied here, $a_\pm^1 = (a_+^1 a_-^1)^{1/2}$. Note also that the mean activity coefficient of the annealed electrolyte in the limit $c_1 \to 0$ for $T_0 = T_1$ is equal to the mean activity coefficient of the hypothetical fully annealed matrix fluid.[16,23]

A set of results for $\Phi_\pm$, as a function of c_0, is shown in Figure 2. The matrix is prepared from an electroneutral combination of positive and negative ions with $\sigma_+^0 = \sigma_-^0 = 4.25$ Å. We see that at small matrix densities $\Phi_\pm$ becomes higher than unity and falls below this value for more concentrated matrices (larger c_0). This behavior is a clear manifestation of the role of electrostatic attraction between matrix and fluid particles. The results shown by the full line apply to $T_1 = T_0 = 298.15$ K. The influence of the temperature of matrix preparation T_0 can be inferred from the same figure. The result for $T_0 = 148.15$ K ($T_1 = 298.15$ K and remains unchanged) is shown by the dashed line. Due to stronger electrostatic interaction between matrix particles, the oppositely charged matrix ions encounter each other on average at smaller distances (cf. Figure 1b) than at $T_0 = 298.15$ K. In this way, the matrix ions are better screened mutually and consequently electrostatic effects of the matrix on $\Phi_\pm$ are less pronounced. This yields a weaker affinity of fluid ions to matrix particles and stronger "excluded volume" effects. Next, we present a similar calculation for *NaCl* solution introduced into the matrix at $T_0 = T_1 = 298.15$ K (dotted line). Due to the smaller radius of the sodium ion, $\sigma_{Na} = 3.87$ Å in comparison with the lithium ion ($\sigma_{Li} = 5.43$ Å), its attraction with negative charges of the matrix is stronger, which is reflected in higher values of $\Phi_\pm$. At the end we show the $\Phi_\pm$ values for model *LiCl* adsorption in a matrix ($\sigma_+^0 = \sigma_-^0 = 4.25$ Å), where the matrix "ions" are striped of their charge. As expected, these results are shown by symbols; $\Phi_\pm$ for such a hard-sphere matrix decreases with increasing matrix concentration.

In addition to the matrix concentration and conditions of its preparation, the temperature of adsorption T_1 has a strong influence on the $\Phi_\pm$ values. This is illustrated in Figure 3. where the result of trace *LiCl* adsorption at three different values of T_1 are presented. The continuous line applies to $T_1 = 298.15$ K, the dashed line to 198.15 K, and the dotted line to 148.15 K. In all three cases $T_0 = 298.15$ K. It is evident that by decreasing the temperature of adsorption the fluid−matrix attraction becomes stronger, and consequently electrostatic effects dominate, making $\Phi_\pm$ values larger than unity over a wide region of matrix densities. In summary, the thermodynamic parameters that influence the affinity of the model electrolyte to a given matrix are the matrix concentration, conditions of its preparation, and the actual temperature of adsorption.

6.2. Excess Internal Energy. The excess internal energy of an electrolyte inside a charged matrix has been extensively studied in our previous papers,[20,21,24] and is not of primary interest in the present study. In Figure 4 we show the results for the reduced (divided by $k_B T_1$) excess internal energy per fluid particle corresponding to the model *LiCl* electrolyte as a function of its mean activity $a_\pm^1$. The temperature of matrix preparation, T_0, and the temperature of adsorption, T_1, were both set to 298.15 K in this calculation. As in all other examples studied here the matrix ions were assumed to be equal-sized charged spheres with diameters $\sigma_+^0 = \sigma_-^0 = 4.25$ Å. Matrices of different concentration were examined: the dashed curve in Figure 4 (no symbols) applies to bulk electrolyte, and the curves with symbols (top to bottom) belong to matrix concentrations

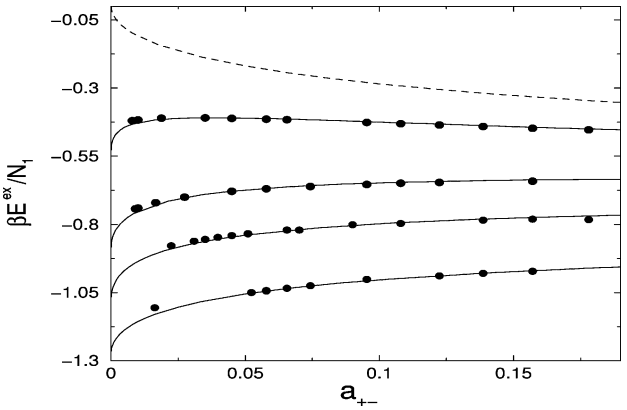

Figure 4. Reduced excess internal energy of adsorbed *LiCl* solution per particle as a function of $a_{\pm}^1$. The dashed line (no symbols) represents results for bulk *LiCl* solution. The continuous curves denote results of the ROZ/HNC theory, from top to bottom: $c_0 = 0.1$, 0.5, 1.0, and 2.0 mol/dm^3. The symbols are results of the grand canonical Monte Carlo simulation. Other parameters: $T_1 = T_0 = 298.15$ K, $\sigma_+^0 = \sigma_-^0 = 4.25$ Å.

$c_0 = 0.1$, 0.5, 1.0, and 2.0 mol/dm^3. In agreement with previous studies, we may conclude that the matrix medium has a strong influence on the excess internal energy of the adsorbed fluid. As expected, this influence is stronger for more concentrated matrices. Also, as discussed previously,[20,21,24] due to the Coulombic nature of the interaction, the excess internal energy is quite sensitive to the dielectric constant and temperature of the annealed electrolyte. The agreement between the ROZ/HNC theory and computer simulations (symbols) is good.

6.3. Adsorption Isotherms. In analogy with previous studies,[22,23] it is assumed that the adsorbed electrolyte of concentration c_1 is in thermodynamic equilibrium with an external electrolyte solution. This means that the chemical potentials of all mobile ions and solvent in the microporous phase must be equal to those in the external electrolyte of the same chemical composition. In Figure 5 the concentration of adsorbed electrolyte is given as a function of the mean activity, $a_{\pm}^1 = (a_+^1 a_-^1)^{1/2} = \gamma_{\pm}^1 c_1$. Several isotherms are shown: the continuous curves from top to bottom belong to matrices with $c_0 = 0.5$, 1.0, and 2.0 mol/dm^3, respectively. The results for an equilibrium bulk electrolyte are shown by the dashed lines (no symbols attached). Again, the symbols denote the grand canonical Monte Carlo data.

Let us discuss first Figure 5a, where the results apply to $T_0 = T_1 = 298.15$ K. It is evident that the mean activity coefficient $\gamma_{\pm}^1$ for model *LiCl* in the matrix is higher than the same quantity in the equilibrium external electrolyte. In other words, the electrolyte solution is "excluded" from the matrix under these conditions; its equilibrium concentration in the matrix, c_1, is lower than that in the equilibrium outside solution with the same value of $a_{\pm}^1$. The exclusion is stronger for more concentrated matrices, and this is a consequence of the excluded volume. This kind of behavior is in accordance with the results for $\Phi_{\pm}(c_0)$ given in Figure 2, and has already been observed in previous calculations.[22,23,25]

A qualitatively different picture emerges at low temperatures of adsorption. In Figure 5b we present calculations for the same electrolyte−matrix system as above, except that the temperature of observation T_1 is 148.15 K. All other parameters remain unchanged and the notation is as for the previous figure: the ROZ/HNC results for adsorbed electrolytes are shown by the continuous lines, the HNC results for the equilibrium bulk electrolyte with the dashed line, and the grand canonical Monte

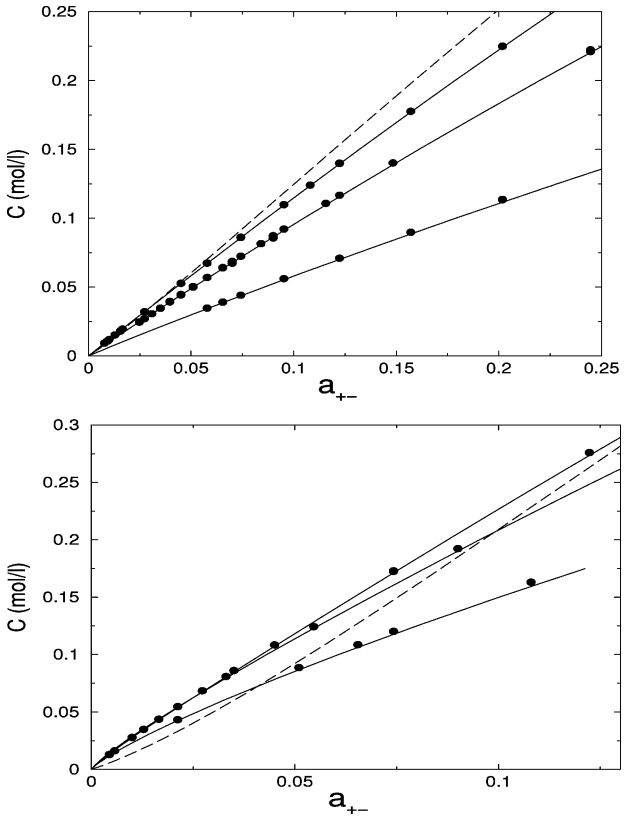

Figure 5. Adsorption isotherms (continuous lines with symbols) for *LiCl* model electrolyte in matrices of different concentration (from top to bottom): $c_0 = 0.5$, 1.0, and 2.0 mol/dm^3. The dashed line with no symbols attached shows the results for bulk electrolyte. The symbols denote the grand canonical Monte Carlo results. Panel a (top): $T_1 = T_0 = 298.15$ K. Panel b (bottom): $T_1 = 148.15$ K and $T_0 = 298.15$ K. In all cases $\sigma_+^0 = \sigma_-^0 = 4.25$ Å.

Carlo results by symbols. Note that for $T_1 = 148.15$ K the electrostatic interactions between fluid ions, as well as between fluid and matrix ions, are approximately twice as strong as in the previous case, where $T_1 = 298.15$ K. The matrix is prepared at $T_0 = 298.15$ K, so this situation applies to the case where $\epsilon_0 T_0/\epsilon_1 T_1 > 1$ discussed in detail in ref 16. In such a situation an annealed ion will, on average, find itself in configurations such that an opposite charge exceeds its own charge (see, for example, Figure 8 of ref 19). As a consequence, one may expect the competition between adsorption of fluid ions on the matrix particles (see Figure 3, dotted curve), on one hand, and the screened interactions between the annealed ions, on the other. Altogether, the situation here is much more complex than for Figure 5a, and the mean activity coefficient of the adsorbed electrolyte can be larger or smaller than the same quantity in the external equilibrium solution. For strong couplings (low values of T_1), and concentrations of all species that are not too high, we may have sorption of the electrolyte into the matrix and not exclusively rejection, as for the example shown in Figure 5a. More precisely, in the region of small c_1, there is sorption of electrolyte for all three matrix concentrations studied. For minute amounts of adsorbed electrolyte the sorption is, in accordance with Figure 3, the highest for a matrix with $c_0 = 1.0$ mol/dm^3. Over a wider range of activities, however, the strongest adsorption is observed for a matrix with c_0 equal to 0.5 mol/dm^3. With increasing activity of the external electrolyte there is a change in "sign" of the adsorption. For all three matrices (lines with symbols), there is a concentration where these lines cross the "bulk curve" (dashed line). For such a point

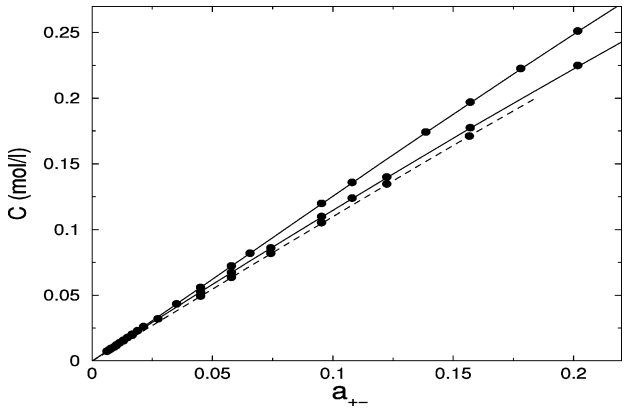

Figure 6. Adsorption isotherms for *LiCl* at $T_1 = 298.15$K: (a) $T_0 = 298.15$ K, matrix with $c_0 = 0.1$ mol/dm^3 (top full curve), and $c_0 = 0.5$ mol/dm^3 (lower continuous curve); (b) $T_0 = 148.15$ K, $c_0 = 0.5$ mol/dm^3 (dashed line). As before the symbols denote the grand canonical Monte Carlo results.

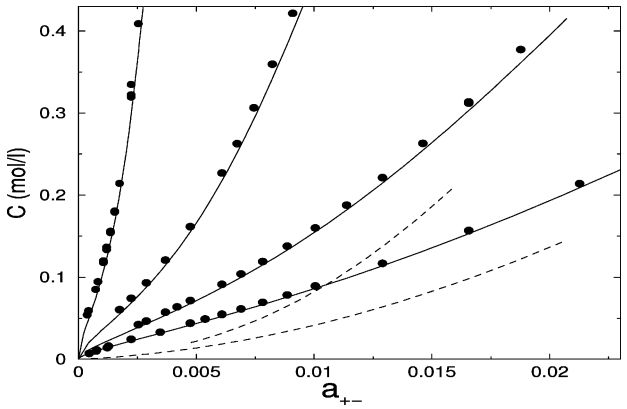

Figure 7. Adsorption isotherms for *LiCl* at various temperatures of observation T_1; $c_0 = 0.1$ mol/dm^3, $T_0 = 298.15$ K. Legend, top to bottom: $T_1 = 40.15$, 50.15, 60.15, and 70.15 K. The symbols denote the grand canonical Monte Carlo data as before. The dashed lines apply to bulk electrolyte at $T_1 = 60.15$ K (upper curve) and $T_1 = 70.15$ K (lower curve).

the concentration of adsorbed electrolyte is exactly equal to the concentration of external equilibrium solution. Note that the position of the crossover point is shifted toward smaller values of $a_\pm$ with increasing values of c_0. It is clear from these pictures that ROZ/HNC predictions agree very well with the computer simulations.

In the next example, Figure 6, we consider two matrices of the same concentration $c_0 = 0.5$ mol/dm^3, but one of them was prepared at $T_0 = 298.15$ K (lower continuous line) and the other at $T_0 = 148.15$ K (dashed line). The Monte Carlo results, depicted by symbols, follow the ROZ/HNC lines very well. The temperature of observation is $T_1 = 298.15$ K. The difference in structure between the two matrices is shown in Figure 1b. Stronger electrostatic interactions in the latter case ($T_0 = 148.15$ K) result in a higher probability of contact between oppositely charged matrix ions, as well as in a shorter range of correlations compared to the matrix prepared at $T_0 = 298.15$ K. As a result of better screening between the matrix ions when prepared at lower temperature, such a matrix has a smaller adsorption capacity. This again is in accordance with the $\Phi_\pm$ calculations shown in Figure 2. The effect of variation of T_0 is, however, very small under these conditions. In the same figure we present the results for $c_0 = 0.1$ mol/dm^3 (top continuous line). In this case the effect of T_0 is even smaller and, due to the low matrix concentration, the adsorption isotherms for both temperatures are very close to each other, and therefore only the results for $T_0 = 298.15$ K are shown.

In Figure 7, the results for an electrolyte confined to a matrix with concentration $c_0 = 0.1$ mol/dm^3 and prepared at $T_0 = 298.15$ K are given. In this example the temperature of observation T_1 is the parameter. These results correspond from top to bottom to $T_1 = 40.15$, 50.15, 60.15, and 70.15 K. For all the temperatures studied here the replica OZ equation in the HNC approximation can be solved without difficulty. In other words, we did not encounter any convergence problems though, however, some patience is needed in solving the set ROZ integral equations. In the same figure (dashed lines) we present the results for the bulk electrolyte as obtained by the regular OZ/HNC approach. Convergent solutions for $T_1 = 70.15$ K (lower dashed line) can be obtained over the whole concentration range. For $T_1 = 60.15$ K (upper dashed line) there is a region of low concentrations where the HNC approximation fails to converge. One can see from this plot that the concentration of adsorbed electrolyte in the matrix is considerably larger than the bulk fluid concentration. For this low temperature there is a large intake of electrolyte by the matrix. This means that the mean activity coefficient of the adsorbed electrolyte is lower (influence of the matrix-annealed fluid interaction) than the same quantity in the equilibrium bulk solution. Note that no convergent solution of the OZ/HNC for the bulk electrolyte could be obtained for the two lowest temperatures $T_1 = 50.15$ and 40.15 K. The agreement between the ROZ/HNC theory and our grand canonical Monte Carlo results is reasonably good even for low temperatures.

6.4. Isothermal Compressibility. In the next figures we present the ROZ/HNC results for the reduced isothermal compressibility$[\partial\rho_1/\partial(\beta_1 P)]_T$ of the adsorbed fluid as a function of the mean activity. Note that eq 14 calculates the reciprocal values to this quantity. The isothermal compressibility is related to the fluctuations of the fluid particle number about its average value.[8] In this way a large increase of isothermal compressibility reflects a possible instability of the observed system. Unfortunately, the accuracy of the concentration fluctuation results, as obtained by the grand canonical Monte Carlo simulation, is relatively low and very long runs are needed to smooth out the fluctuations in this quantity. For this reason, no comparison between the ROZ/HNC and grand canonical simulation results for the isothermal compressibility is presented.

In Figure 8 we show results for the ROZ/HNC isothermal compressibility, calculated with the help of eq 14, for a model *LiCl* solution at four different matrix concentrations. The curve connecting symbols (*) belong to $c_0 = 0.1$ mol/dm^3, filled circles belong to a matrix with $c_0 = 0.5$ mol/dm^3, and the lines with squares and triangles denote the results for $c_0 = 1.0$ and 2.0 mol/dm^3, respectively. The model parameters correspond to results for the adsorption isotherm shown in Figure 5 and discussed in the preceding section.

The results for isothermal compressibility at $T_1 = T_0 = 298.15$ K are plotted in Figure 8a as a function of the mean activity of annealed electrolyte. The compressibility curve for an unperturbed model *LiCl* solution is shown in Figure 8a by a continuous line with no symbols attached.[32] In the bulk electrolyte the increase of compressibility above the ideal value is attributed to the attractive long-range correlations between the ions before an excluded volume effect begins to have influence. For a low concentration matrix ($c_0 = 0.1$ mol/dm^3) the behavior is qualitatively similar to that of symmetric bulk electrolytes. The attractive electrostatic forces yield to increased compressibility in the low activity region, while for higher $a_\pm^1$

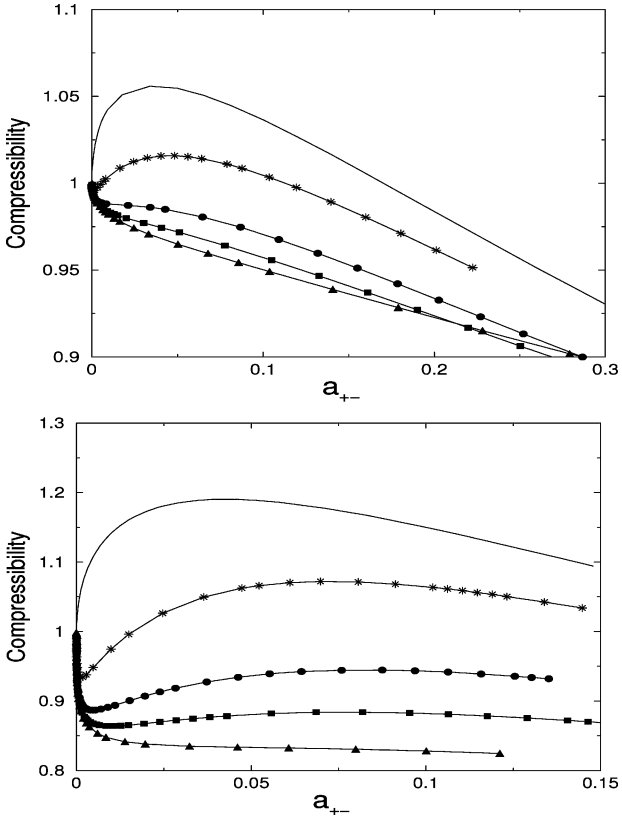

Figure 8. Isothermal compressibility results for *LiCl* model electrolyte in matrices of different concentration: $c_0 = 0.5$ (circles), 1.0 (squares), and 2.0 mol/dm^3 (triangles). Panel a (top): $T_1 = T_0 = 298.15$ K. Panel b (bottom): $T_1 = 148.15$ K and $T_0 = 298.15$ K. The curves for $c_0 = 0.1$ mol/dm^3 are shown by a solid line with stars. The continuous line with no symbols attached shows the results for bulk electrolyte.

values the compressibility decreases. Even for this very dilute matrix the value of the maximum compressibility is substantially depressed compared to that of the bulk electrolyte. In general, the effect of matrix concentration is such that it decreases the isothermal compressibility for all values of the mean activity.

In contrast to results for $c_0 = 0.1$ mol/dm^3, the compressibility curves calculated for other matrix concentrations (0.5, 1.0, and 2.0 mol/dm^3) do not exhibit a maximum under these conditions where electrostatic interactions are relatively weak. For these matrices the compressibility decreases from the ideal value, indicating that the presence of obstacles strongly suppresses the concentration fluctuations in these systems. The immediate decrease of compressibility seems to be a combined effect of matrix density on one hand and the adsorption of fluid ions on matrix particles on the other. For example, in the most concentrated matrix, $c_0 = 2.0$ mol/dm^3 studied in this work, the adsorbed fluid concentration is low. The annealed fluid ions are to a large extent adsorbed on, or better stated attached, to the matrix ions. As a result the compressibility value is low. For the dilute matrix where $c_0 = 0.1$ mol/dm^3, with a much lower number of adsorbing obstacles, the concentration of adsorbed fluid is higher (cf. Figure 5a) for a given mean activity of the external solution. Some of the annealed ions are attached to adsorbing centers, but the remaining ions may correlate via attractive electrostatic forces, and the resulting value of the compressibility is higher than that in the denser matrix where $c_0 = 1.0$ mol/dm^3. In other words, the shape of the compressibility curve reflects to what degree the electrostatic interactions characteristic of the bulk electrolyte are perturbed by the presence of obstacles.

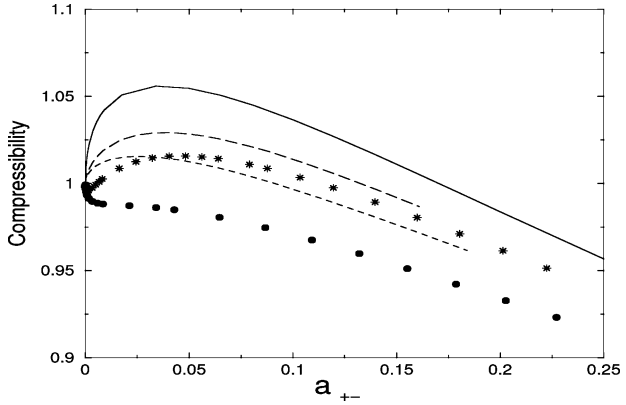

Figure 9. Isothermal compressibility results for *LiCl* model solution at $T_1 = 298.15$ K: (a) $T_0 = 298.15$ K, matrix with $c_0 = 0.5$ (circles) and 0.1 mol/dm^3 (stars); (b) $T_0 = 148.15$ K, $c_0 = 0.5$ (short dashed line) and 0.1 mol/dm^3 (long dashed line). The continuous line represents the results for bulk electrolyte at 298.15 K.

For adsorption performed at a lower temperature, shown in Figure 8b, where $T_1 = 148.15$ K, the electrostatic interactions are stronger and their consequences more complex. The isothermal compressibility, plotted as a function of $a_{\pm}$, after an initial drop, increases and after reaching the maximum, it decreases again. For $c_0 = 0.1$ mol/dm^3 the calculated values of the isothermal compressibility at $T_1 = 148.15$ K are higher than those obtained for $T_1 = 298.15$ K (Figure 8a). In contrast to this result, the compressibility of the same electrolyte in a dense matrix ($c_0 = 2.0$ mol/dm^3) is lower at $T_1 = 148.15$ K than at higher temperature. The result for the bulk electrolyte solution is presented by the continuous line with no symbol.

The effect on the electrolyte compressibility of matrix preparation (T_0 dependence) is shown in Figure 9. This figure describes the situation previously studied in terms of the electrolyte adsorption, with the results shown in Figure 6. We consider two matrices of concentration $c_0 = 0.5$ mol/dm^3 and at $T_1 = 298.15$ K. One of the matrices is prepared at $T_0 = 298.15$ K (these results are shown by circles), and the other at $T_0 = 148.15$ K (short dashed line). The pair-correlations in the two matrices are discussed in relation to Figure 1b. In addition, we show similar results for a much less concentrated matrix with $c_0 = 0.1$ mol/dm^3. The results, obtained for $T_0 = 298.15$ K, are denoted by symbols *, and the results for the lower temperature $T_0 = 148.15$ K by the long dashed line. For adsorption in a dilute matrix ($c_0 = 0.1$ mol/dm^3) the compressibility curves exhibit a maximum, which is higher for lower values of T_0. For comparison, the result for a bulk electrolyte solution is shown by a continuous line.

The compressibility results presented in Figure 9 can be explained in terms of the electrostatic interactions between the annealed ions, and annealed ions and matrix particles. As seen in Figure 1b the correlations between ions in a matrix prepared at $T_0 = 148.15$ K are of shorter range than for those quenched at $T_0 = 298.15$ K. In simple terms, the matrix influence on annealed ions is weaker if it is prepared at lower temperature. In this way the compressibility values for the fluid adsorbed in a colder matrix (long dashed line) are higher compared to the "warmer" matrix prepared at $T_0 = 298.15$ K (stars). The same explanation applies to results for matrix concentration $c_0 = 0.5$ mol/dm^3, shown in the same figure. Note that the influence of variation of T_0 on the adsorption isotherm is much smaller than that observed here (cf. Figure 6).

The compressibility results shown in Figure 10 are obtained for the same conditions and values of parameters as the

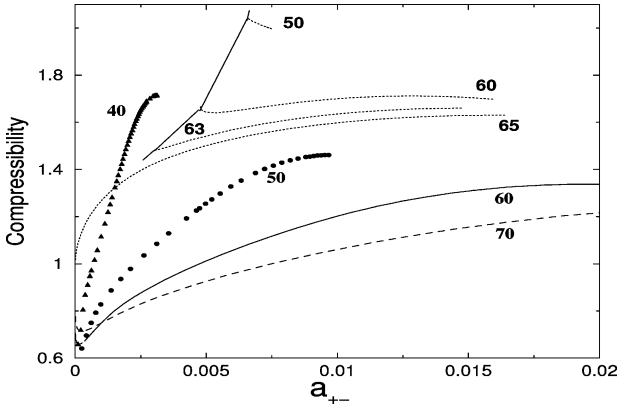

Figure 10. Isothermal compressibility for *LiCl* model solution at various temperatures of observation T_1 as indicated in the figure. The dotted lines are calculated for bulk electrolyte solution and the continuous vertical lines connecting dotted curves indicate the points where the ROZ/HNC solution is lost; $c_0 = 0.1$ mol/dm^3, $T_0 = 298.15$ K.

adsorption isotherms presented in Figure 7. In this way the compressibility data complement the previous adsorption results. The results are, as in other figures, plotted as a function of the mean activity of annealed electrolyte. The dotted lines apply to bulk electrolyte solutions (no matrix present) and are obtained by using the regular OZ/HNC approximation. The temperatures of observation T_1, measuring the strength of electrostatic coupling, are indicated on the figure. If we start to build the T_1 isotherm at some high enough value of the mean activity of adsorbed electrolyte and then decrease $a_{\pm}^1$ we may encounter convergence problems. At a certain value of the mean activity, and for a low enough value of T_1, we may lose the numerical solution. That is why the plots shown in this figure are not complete; the vertical lines connecting the dotted lines show the values of $a_{\pm}^1$ where the algorithm stopped converging. The numerical solution usually reappears for extremely low electrolyte concentrations, but these results, for the sake of clarity of presentation, are not shown in the figure. The lowest temperature at which we have obtained a solution over the entire range is $T_1 = 65.15$ K. On the other hand, for an electrolyte adsorbed in a matrix of concentration $c_0 = 0.1$ mol/dm^3 and prepared at $T_0 = 298.15$ K, convergent results can be obtained for much lower temperatures such as $T_1 = 50.15$ and 40.15 K. We have not attempted to obtain solutions at even lower temperatures, nor to trace the range of solvability of the ROZ/HNC algorithm. Note that electrostatic interaction between the annealed ions and ionic obstacles is very strong in dilute matrices, as is also documented in Figures 2 and 3. These calculations are quite time-consuming and a more systematic investigation for the matrices characterized by other c_0 and T_0 values has to be postponed for future contributions.

7. Conclusions

In this paper we present the replica Ornstein−Zernike and grand canonical Monte Carlo results for a simple partly quenched system. The matrix subsystem is formed at temperature T_0 from a charge and size symmetric +1:−1 primitive model electrolyte of concentration c_0 and of dielectric constant ϵ_0. The annealed electrolyte is another primitive model +1:−1 electrolyte, characterized by a dielectric constant ϵ, and with ionic diameters to mimic *LiCl* solution. The annealed electrolyte, distributed within the matrix subsystem at temperature T_1 and ϵ, is assumed to be in thermodynamic equilibrium with an external electrolyte solution of the same chemical composition. The quantities of primary interest for this study were the chemical potential (mean activity) of the adsorbed electrolyte and the isothermal compressibility. The adsorption and compressibility isotherms are determined by varying the matrix density, temperature of preparation, and other model parameters. In the present study, we were particularly interested in the low-temperature behavior of the replica OZ/HNC approach. An attempt was made to investigate the adsorption of the model electrolyte in charged matrices under the condition of strong coupling, and to compare the observed trends with the corresponding results for the bulk-electrolyte OZ/HNC calculations and with a new batch of computer simulations. The adsorption isotherms calculated via the ROZ/HNC theory agree well with the grand canonical Monte Carlo results.

Since 1968, when the paper by Stillinger and Lovett[35] was published, there has been strong evidence that a fluid of charged hard spheres undergoes a phase transition, analogous to the liquid−gas transition.[36,37] Very useful information about the region of coexistence has been obtained from computer simulations.[38−41] On the other hand, the HNC approximation is not well suited for these problems. An extensive analysis of the behavior of the HNC integral equation near the two-phase region has been performed by Belloni.[30] He showed that the HNC equation has no solution inside a certain region of parameters whose boundary line is not a spinodal line. As this boundary is approached, the isothermal compressibility does not diverge. The behavior of the OZ/HNC approximation is universal, and applies to very different interparticle pair potentials, not only to the primitive model electrolytes. Our observations, based on numerous calculations, suggest that the same behavior applies to the present replica OZ/HNC approximation. In other words, not getting a convergent solution does not necessarily mean that we are at the spinodal line.

Theoretical studies[42] and computer simulations[40] suggest that for the restrictive primitive model the fraction of free ions is negligible in the vicinity of the coexistence region. In this way, the equilibrium properties of the system are mostly determined by the neutral clusters present in solution, and free ions represent merely a perturbation. Returning now to the electrolyte adsorbed in the disordered matrix, it seems plausible to assume that the matrix "stabilizes" an adsorbed electrolyte if its effect is such to inhibit the cation−anion pair formation. The matrix in this study is modeled as a charge and size symmetric +1:−1 primitive model electrolyte. It is clear that such a matrix will not promote pair-formation. If a cation and anion of the annealed fluid are introduced into such a material, the cation will try to bind to a negatively charged obstacle and the anion to a positively charged obstacle. This will occur with greater probability if the ions in adsorbed solution are fewer than the matrix charges. In any case, oppositely charged pair-formation is suppressed and we may expect a decrease of the critical temperature under such conditions. The situation, however, may be qualitatively different for dense neutral matrices: due to space limitations pair-formation will be favored in this case. One may speculate that adsorption, as well as the critical behavior of the adsorbed electrolyte, may be governed by the changing composition of the matrix composed of neutral and charged species. We conclude with the observation that, at present, there is no integral equation theory able to describe quantitatively the phase transitions in charged systems with quenched disorder. We believe that computer simulations may represent an adequate tool to solve this problem soon.

Acknowledgment. This work was supported in part by DGAPA of the National University of Mexico (UNAM) under

Grant No. IN113201 and CONACyT of Mexico under Grant No. 37323E. V.V. acknowledges the support of the Ministry of Education, Science and Sport of the Republic of Slovenia (Grant No. 103-505).

References and Notes

(1) Madden, W. G.; Glandt, E. D. *J. Stat. Phys.* **1988**, *51*, 537.
(2) Madden, W. G. *J. Chem. Phys.* **1992**, *96*, 5422.
(3) Given, J. A.; Stell, G. *J. Chem. Phys.* **1992**, *97*, 4753.
(4) Given, J. A.; Stell, G. *Physica A* **1994**, *209*, 495.
(5) Given, J. A. *J. Chem. Phys.* **1995**, *102*, 2934.
(6) Tatlipinar, H.; Pastore, G.; Tosi, M. P. *Philos. Mag. Lett.* **1993**, *68*, 357.
(7) Lomba, E.; Given J. A.; Stell, G.; Weis, J. J.; Levesque D. *Phys. Rev. E* **1993**, *48*, 233.
(8) Rosinberg, M. L.; Tarjus, G.; Stell, G. *J. Chem. Phys.* **1994**, *100*, 5172.
(9) Ford, D. M.; Glandt, E. D. *J. Chem. Phys.* **1994**, *100*, 2391.
(10) Meroni, A.; Levesque, D.; Weis, J. J. *J. Chem. Phys.* **1996**, *105*, 1101.
(11) Kierlik, E.; Rosinberg, M. L.; Tarjus, G.; Monson, P. A. *J. Chem. Phys.* **1997**, *106*, 264.
(12) Pizio, O.; Sokolowski, S. *J. Phys. Stud.* **1998**, *2*, 296.
(13) Rosinberg, M. L. In *New Approaches to Problems in Liquid-State Theory*; Caccamo, C., Hansen, J.-P., Stell, G., Eds.; Kluwer: Dordrecht, The Netherlands, 1999; p 245.
(14) Pizio, O. In *Computational Methods in Surface and Colloid Science*; Borowko, M., Ed.; Marcel Dekker: New York, 2000; p 293.
(15) Bratko, D.; Chakraborty, A. K. *Phys. Rev. E* **1995**, *51*, 5805.
(16) Bratko, D.; Chakraborty, A. K. *J. Chem. Phys.* **1996**, *104*, 7700.
(17) Chakraborty, A. K.; Bratko, D.; Chandler, D. *J. Chem. Phys.* **1994**, *100*, 1528.
(18) Deem, M. W.; Chandler, D. *J. Stat. Phys.* **1994**, *76*, 911.
(19) Hribar, B.; Pizio, O.; Trokhymchuk, A.; Vlachy, V. *J. Chem. Phys.* **1997**, *107*, 6335.
(20) Hribar, B.; Pizio, O.; Trokhymchuk, A.; Vlachy, V. *J. Chem. Phys.* **1998**, *109*, 2480.
(21) Hribar, B.; Vlachy, V.; Pizio, O.; Trokhymchuk, A. *J. Phys. Chem. B* **1999**, *103*, 5361.
(22) Hribar, B.; Vlachy, V.; Pizio, O. *J. Phys. Chem. B* **2001**, *105*, 4727.
(23) Hribar, B.; Vlachy, V.; Pizio, O. *Mol. Phys.* **2002**, *100*, 3093.
(24) Hribar, B.; Vlachy, V.; Pizio, O. *J. Phys. Chem. B* **2000**, *104*, 4479.
(25) Dominguez, H.; Hribar, B.; Vlachy, V.; Pizio, O. *Physica A* **2003**, *424*, 471.
(26) Simonin, J. P.; Bernard, O.; Blum, L. *J. Phys. Chem.* **1998**, *102*, 4411.
(27) Ramanathan, P. S.; Friedman, H. L. *J. Chem. Phys.* **1971**, *54*, 1086.
(28) Rasaiah, J. C. In *The Liquid States and its Electrical Properties*; Kunhardt, E. E., Christophorou, L. G., Luessen, L. H., Eds.; N.A.T.O. ASI Ser. B; Plenum Press: New York, 1988; Vol. 193.
(29) Vlachy, V. *Annu. Rev. Phys. Chem.* **1999**, *502*, 145.
(30) Belloni, L. *J. Chem. Phys.* **1993**, *98*, 8080.
(31) Friedman, H. L.; Dale, W. D. T. *Statistical Mechanics, Part A*: *Equilibrium Techniques*; Part of Vol. 5 of Modern Theoretical Chemistry; Berne, B. J., Ed.; Plenum: New York, 1977.
(32) Vlachy, V.; Ichiye, T.; Haymet, A. D. J. *J. Am. Chem. Soc.* **1991**, *113*, 1077.
(33) Hansen, J. P.; McDonald, I. R. *Theory of Simple Liquids*; Academic: London, UK, 1986.
(34) Van Tassel, P. R. L. *Phys. Rev.* **1999**, *60*, R25.
(35) Stillinger, F. H.; Lovett, R. *J. Chem. Phys.* **1968**, *48*, 3858.
(36) Stell, G. *J. Stat. Phys.* **1995**, *78*, 197.
(37) Fisher, M. E. *J. Phys. Condens. Matter* **1996**, *8*, 9103.
(38) Graham, I. S.; Valleau, J. P. *J. Phys. Chem.* **1990**, *94*, 7894.
(39) Panagiotopulos, A. Z. *J. Chem. Phys.* **2002**, *116*, 3007.
(40) Romero-Enrique, J. M.; Rull, R. F.; Panagiotopulos, A. Z. *Phys. Rev. E* **2002**, *66*, 041204.
(41) Yan, Q.; de Pablo, J. J. *Phys. Rev. Lett.* **2002**, *88*, 095504.
(42) Jiang, J. W.; Blum, L.; Bernard, O.; Prausnitz, J. M.; Sandler, S. I. *J. Chem. Phys.* **2002**, *116*, 7977.